

# XMM-Newton and Chandra observations of SHEEP sources

I. Georgantopoulos<sup>1</sup>, K. Nandra<sup>2</sup>, M. Brotherton<sup>3,4</sup>, A. Georgakakis<sup>1,2</sup>, I. E. Papadakis<sup>5</sup>, P. O’Neill<sup>2</sup>

<sup>1</sup>*Institute of Astronomy & Astrophysics, National Observatory of Athens, I. Metaxa & V. Pavlou, Athens, 15236, Greece*

<sup>2</sup>*Astrophysics Group, Imperial College London, Blackett Laboratory, Prince Consort Rd, SW7 2AW*

<sup>3</sup>*Department of Physics & Astronomy, University of Wyoming, Laramie, WY82071, USA*

<sup>4</sup>*Kitt Peak National Observatory, 950 N. Cherry Avenue, Tucson, AZ 85719, USA*

<sup>5</sup>*Physics Department, University of Crete, 71003, Heraklion, Greece*

15 October 2018

## ABSTRACT

We present *Chandra* and *XMM-Newton* observations of 12 bright ( $f(2\text{--}10\text{keV}) > 10^{-13}$  erg cm<sup>-2</sup> s<sup>-1</sup>) sources from the *ASCA* SHEEP (Search for the High Energy Extragalactic Population) survey. Most of these have been either not observed or not detected previously with the *ROSAT* mission and therefore they constitute a sample biased towards hard sources. The *Chandra* observations are important in locating with accuracy the optical counterpart of the X-ray sources. Optical spectroscopic observations show that our sample is associated with both narrow-line (NL) (six objects), and Broad-Line (BL) AGN (five objects) with one source remaining unidentified. Our sources cover the redshift range 0.04 to 1.29 spanning luminosities from 10<sup>42</sup> to 10<sup>45</sup> erg s<sup>-1</sup> (2-10 keV). The NL sources have preferentially lower redshift (and luminosity) compared with the BL ones. This can be most easily explained in a model where the NL AGN are intrinsically less luminous than the BL ones in line with the results of Steffen et al. The X-ray spectral fittings show a roughly equal number of obscured ( $N_H > 10^{22}$  cm<sup>-2</sup>) and unobscured ( $N_H < 10^{22}$  cm<sup>-2</sup>) sources. There is a clear tendency for obscured sources to be associated with NL AGN and unobscured sources with BL ones. However, there is a marked exception with the highest obscuring column observed at a BL AGN at a redshift of  $z=0.5$ .

**Key words:** Galaxies: active – Quasars: general – X-rays: general

## 1 INTRODUCTION

*Chandra* surveys resolved 80 per cent of the X-ray background at hard energies (i.e. 2-10 keV) Brandt et al. (2002), Giacconi et al. (2002), Alexander et al. (2003), shedding ample light on its origin. Optical identifications of the X-ray sources are showing that these are mainly AGN. The largest fraction of these are absorbed in X-rays, presenting an average spectrum with a slope of  $\Gamma = 1.4$  (Tozzi et al. 2001) similar to the slope of the X-ray background. Large area bright surveys performed with XMM-Newton in the 2-10 keV band are complementary as they help us to explore the bright, nearby counterparts of the sources detected in the deep *Chandra* fields. One remarkable finding from these bright surveys is the scarcity of obscured AGN ( $N_H > 10^{22}$  cm<sup>-2</sup>) at bright fluxes (Piconcelli et al. 2002, Georgantopoulos et al. 2004, Perola et al. 2004). This comes in contrast to the predictions of the population synthesis models (e.g. Comastri et al. 1995, Gilli et al. 2001).

Selection in the hardest band allowed by imaging sur-

veys (5-10 keV) facilitates the selection of the most obscured candidates, as this bandpass is relatively unbiased to absorption. Indeed columns as high as a few times 10<sup>23</sup> cm<sup>-2</sup> do not practically affect X-ray energies above 5 keV. The HELLAS survey (Fiore et al. 1999) pioneered these studies using the MECS detector on board *BeppoSAX*. The HELLAS survey covered an area of 85 deg<sup>2</sup> detecting about 150 sources down to a flux limit of  $5 \times 10^{-14}$  erg cm<sup>-2</sup> s<sup>-1</sup> in the 5-10 keV band.

The SHEEP survey further explored this energy bandpass with *ASCA* GIS. It comprises of 69 objects serendipitously detected in a non-contiguous area of 39 deg<sup>2</sup> down to a flux limit of  $\sim 10^{-13}$  erg cm<sup>-2</sup> s<sup>-1</sup> in the 5-10 keV band (Nandra et al. 2003). 35 of these objects were detected by *ROSAT*, in either pointed observations or in the All Sky Survey, with 13 of them having secure optical counterparts in optical catalogues. For the remaining 34 sources, which were either not observed or not detected by *ROSAT*, it is very difficult to locate the optical counterpart as the *ASCA*

arXiv:astro-ph/0601245v1 11 Jan 2006

error box is large (typically 60 arcsec rms). We have thus obtained *Chandra* snapshot observations in order to extract reliable positions (<1 arcsec) of the X-ray source that will enable us to search for their optical counterparts. Preliminary results from these observations are presented in Nandra et al. (2004).

Here, we report our results from X-ray and optical observations of 12 out of the 34 *Chandra* sources which have a 2 – 10 keV flux larger than  $10^{-13}$  erg cm $^{-2}$  s $^{-1}$  (estimated assuming a Photon index  $\Gamma = 1.9$ ). We have obtained optical spectroscopy for 11 of these objects. Furthermore, eight of these have been also observed by *XMM-Newton*, providing good quality spectra. Consequently, for these bright sources, we can derive their X-ray spectral parameters (i.e.  $N_H$  and  $\Gamma$ ) using proper spectral fits with good photon statistics (instead of hardness ratios only). Moreover, Nandra et al. (2004) noticed that a fraction of the *Chandra* sources are much fainter (in some cases more than an order of magnitude) than the original *ASCA* source. Although variability could play some role, there is clearly some ambiguity about the reality of these sources. Watanabe et al. (2002) who performed *Chandra* pointings of hard *ASCA* sources also report the same problem. By choosing to study initially only the bright sources, we minimize the possibility that a source is spurious. The optical counterparts for three of the sources in the present SHEEP subsample have already been presented in Nandra et al. (2004). We include them in the present work as they satisfy the flux limit we have set, and we also present the results from *XMM-Newton* observations of them.

## 2 DATA ACQUISITION

### 2.1 The Chandra observations

Our sources were observed using the Advanced CCD Imaging Spectrometer, ACIS-S, on board the *Chandra* observatory (Weisskopf 1997). We use the event file provided by the standard pipeline processing. Only Grade 0,2,3,4 and 6 events are used in the analysis. Charge Transfer Inefficiency (CTI) problems do not affect our observations as S3 is a back-illuminated chip. Each CCD chip subtends an 8.3 arcmin square on the sky while the pixel size is 0.5". The spatial resolution on-axis is 0.5" FWHM. The ACIS-S spectral resolution is  $\sim 100$  eV (FWHM) at 1.5 keV. We estimate that even in the brightest case (AXJ1531.9+2420) the pile-up fraction is less than 12 per cent. Images, spectra, ancillary files, response matrices, and light curves have been created using the CIAO v2.2 software. We use a 2" radius extraction region in order to produce both the spectral files and the light curves. We take into account the degradation of the ACIS quantum efficiency in low energies, due to molecular contamination, by using the ACISABS model in the spectral fitting\*. The observation details are given in Table 1.

### 2.2 The XMM-Newton Observations

The X-ray data have been obtained with the EPIC (European Photon Imaging Camera; Strüder et al. 2001 and Turner et al. 2001) cameras on board the *XMM-Newton*

operating in full frame mode. Four sources have been observed by us while another four have been recovered from the XMM-Newton archive. The observational details are given in Table 2. The data have been analyzed using the Science Analysis Software (SAS 5.3). Event files for both the PN and the MOS detectors have been produced using the EPCHAIN and EMCHAIN tasks of SAS respectively. The event files were screened for high particle background periods. In our analysis we have dealt only with events corresponding to patterns 0-4 for the PN and 0-12 for the MOS instruments.

The source spectra are extracted using an 18 arcsec radius circle. This area includes at least 70 per cent of the X-ray source photons at off-axis angles less than 10 arcmin. The background spectral files are extracted from every image independently, using regions free from sources with a total area about 10 times larger than the source area. The response matrices and the auxiliary files are produced using the SAS tasks RMFGEN and ARFGEN respectively. AXJ1035.1+3938 has just been detected by *XMM-Newton* and thus we cannot derive a spectrum as there are not sufficient counts. The flux of this source is  $F(2 - 10keV) = 6.8 \times 10^{-14}$  erg cm $^{-2}$  s $^{-1}$ .

### 2.3 The optical observations

Optical imaging of our targets in the Johnson B and R band has been performed with the Skinakas 1.3-m/f7.7 Ritchey-Cretien telescope of the University of Crete, except from AXJ0335.2-1505 and AXJ0440.0-4534 which were observed with the ANDICAM detector in the SMARTS 1.3 m telescope at CTIO, Cerro-Tololo Interamerican Observatory. All images were reduced in the same way, as explained by Nandra et al. (2004). Typically, all observations were carried out through standard Johnson *B* and Cousins *R* filters. Exposure time was 20 min for both filters. In all cases, observations were carried out under photometric conditions, with seeing being between  $\sim 1 - 1.5$ -arcsec, and an optical source was detected within 1 arcsec of the *Chandra* source. The first, second, fifth, and the last two sources in Table 3 appear point-like, while the other seven sources are extended, with dimensions ranging between  $\sim 10$  up to  $\sim 30$  arcsec (in the case of AXJ0440.0-4534). The integrated *R*-band magnitudes, and *B - R* colours of all sources are listed in Table 3.

Optical spectroscopy of eight sources in the Northern Hemisphere has been obtained with the Ritchey-Cretien Focus Spectrograph on the 4-m Mayall telescope at the Kitt-Peak National Observatory. The spectral coverage was from 5000 to 8000 Å, with a resolution of about 300 km s $^{-1}$ . The optical spectra for three of these were presented in Nandra et al. (2004). Three more sources have been obtained with the Cassegrain spectrograph at the CTIO 4-m V. N. Blanco telescope on 9 Dec 2003. We used the R-C spectrograph with the G181 grating (316 l/mm), blazed at 7500 Ang, and the order-blocking filter GG-495. There is only one camera-CCD combination that can be used, which is the Loral 3K CCD with the Blue Air Schmidt camera. The slit-width was 1.5" and the spectral resolution was about 250 km/s. The spectral coverage is 5000-9700 Ang. The optical spectra show that five sources present Broad Lines (FWHM > 1000km s $^{-1}$ ) and therefore are clearly associated with AGN. Another six present only Narrow Lines. It is difficult to classify these as in some cases the *H $\alpha$*  or the *H $\beta$*

\* [http://asc.harvard.edu/cal/Acis/Cal\\_prods/qeDeg](http://asc.harvard.edu/cal/Acis/Cal_prods/qeDeg)

name	RA <sup>1</sup>	Dec <sup>1</sup>	Sequence <sup>2</sup>	Exposure <sup>3</sup>	Date
AXJ0140.1+0628	01 40 10.1	+06 28 27	900149	5.8	2002-02-07
AXJ0144.9-0345	01 44 55.4	-03 45 23	900150	4.6	2002-02-07
AXJ0335.2-1505	03 33 18.1	-15 06 17	900152	4.9	2002-02-19
AXJ0440.0-4534	04 40 01.9	-45 34 09	900154	4.7	2002-06-22
AXJ0836.2+5538	08 36 22.8	+55 38 41	900155	4.4	2001-11-10
AXJ1035.1+3938	10 35 15.6	+39 39 09	900158	5.0	2002-03-26
AXJ1230.8+1433	12 30 51.8	+14 33 23	900162	5.2	2002-07-21
AXJ1406.1+2233	14 06 07.0	+22 33 34	900167	4.9	2002-08-05
AXJ1511.7+0758	15 11 49.9	+07 59 19	900172	5.1	2002-07-22
AXJ1531.8+2414	15 31 52.3	+24 14 30	900174	5.5	2002-10-08
AXJ1531.9+2420	15 31 59.0	+24 20 47	900175	5.1	2002-09-25
AXJ1532.5+2415	15 32 33.1	+24 15 26	900177	4.9	2002-07-02

<sup>1</sup> X-ray Equatorial Coordinates J2000; <sup>2</sup> Chandra Sequence number; <sup>3</sup> Exposure in ksec;

**Table 1.** The list of the 12 SHEEP targets studied in this work, and the details of the *Chandra* observations.

Name	Obs-ID	FILTER	PN <sup>1</sup>	MOS <sup>1</sup>	Field name	Date
AXJ0140.1+0628 <sup>+</sup>	0110890901	MED	23.0	26.9	PHL1092	2003-01-18
AXJ0836.2+5538	0143653901	MED	7.1	9.5	AXJ0836.2+5538	2003-10-09
AXJ1035.1+3938 <sup>+</sup>	0109070101	THIN	12.5	15.1	RE1034+396	2002-05-01
AXJ1230.8+1433 <sup>+</sup>	0106060601	THIN	8.9		VIRGO6	2002-07-08
AXJ1406.1+2233 <sup>+</sup>	0051760201	THIN	14.7	17.3	PG1404+226	2001-06-18
AXJ1531.8+2414	0143650101	THIN	4.1	5.9	AXJ1531.9+2420	2003-08-03
AXJ1531.9+2420	0143650101	THIN	4.1	5.9	AXJ1531.9+2420	2003-08-03
AXJ1532.5+2415	0143650101	THIN	4.1	5.9	AXJ1531.9+2420	2003-08-03

<sup>1</sup> Exposure Time in ksec

<sup>+</sup> Archival Observation

**Table 2.** The XMM-*Newton* observations

lines happen to lie outside the spectral window. However, their X-ray properties i.e. high X-ray luminosities ( $L_x > 10^{42}$  erg s<sup>-1</sup>) combined with the hard spectra, suggest that most are AGN. The redshifts and optical classification (BL or NL) are given in Table 3. The spectra are presented in Fig. 1.

### 3 THE DATA ANALYSIS

We investigate the X-ray properties of our sources by performing spectral fittings with the *XSPEC* software package v11.2. The poor count statistics do not allow the use of the standard  $\chi^2$  analysis in all cases. Instead, we use in some cases the C-statistic technique (Cash 1979), which is proper for fitting spectra with limited number of counts. Note that this method can be used to estimate parameter values and confidence regions but does not provide a goodness-of-fit (Arnaud 1996).

We fit the *Chandra* and *XMM-Newton* data separately for each source in the 0.3-8 keV band. In the *XMM-Newton* case we fit simultaneously the PN and the MOS data for each source. We use a power-law model with two absorption components (wa\*zwa\*po in *XSPEC* notation) to fit the data. The column density for the first absorption component is fixed to the Galactic value (the values used for each field were taken from Dickey & Lockman (1990) and are listed in Table 4) while the  $N_H$  for the second com-

ponent (representing the intrinsic absorption) is left as a free parameter during the model fitting process.

In the case of the *Chandra* data where we have limited photon statistics, we fix the photon index to 1.9 and allow both the  $N_H$  and the normalization to vary. In the case of *XMM-Newton* sources with adequate photon statistics we leave both the column density and the photon index free to vary. The results for *Chandra* and *XMM-Newton* are presented in Tables 4 and 5 respectively. All quoted errors correspond to the 90 per cent confidence level. The  $N_H$  values listed in these tables correspond to the column density of the intrinsic component. The luminosities have been estimated assuming  $H_o = 70$ ,  $\Omega_m = 0.3$ ,  $\Omega_\Lambda = 0.7$ . The X-ray spectra are presented in Fig. 2. We see that in some sources that there are residuals which may denote the presence of emission lines. However, in most cases these are hardly statistically significant. The stronger case for a line is in AXJ1531.9+2420, the brightest source in our sample: an FeK line at 6.4 keV (rest-frame) is statistically significant at just above the 95 per cent confidence level. Again a MgXI line at 1.35 keV (rest-frame) is statistically significant at the 93 per cent confidence level.

In the case of those sources where we have many photons to perform a model fitting with the standard  $\chi^2$  analysis, we find that the model fits well the data except from the *Chandra* fits of AXJ1511.7+0758 and AXJ1531.8+2414. The second source has also been observed by *XMM-Newton*, and the model provides a good fit to the data. The best

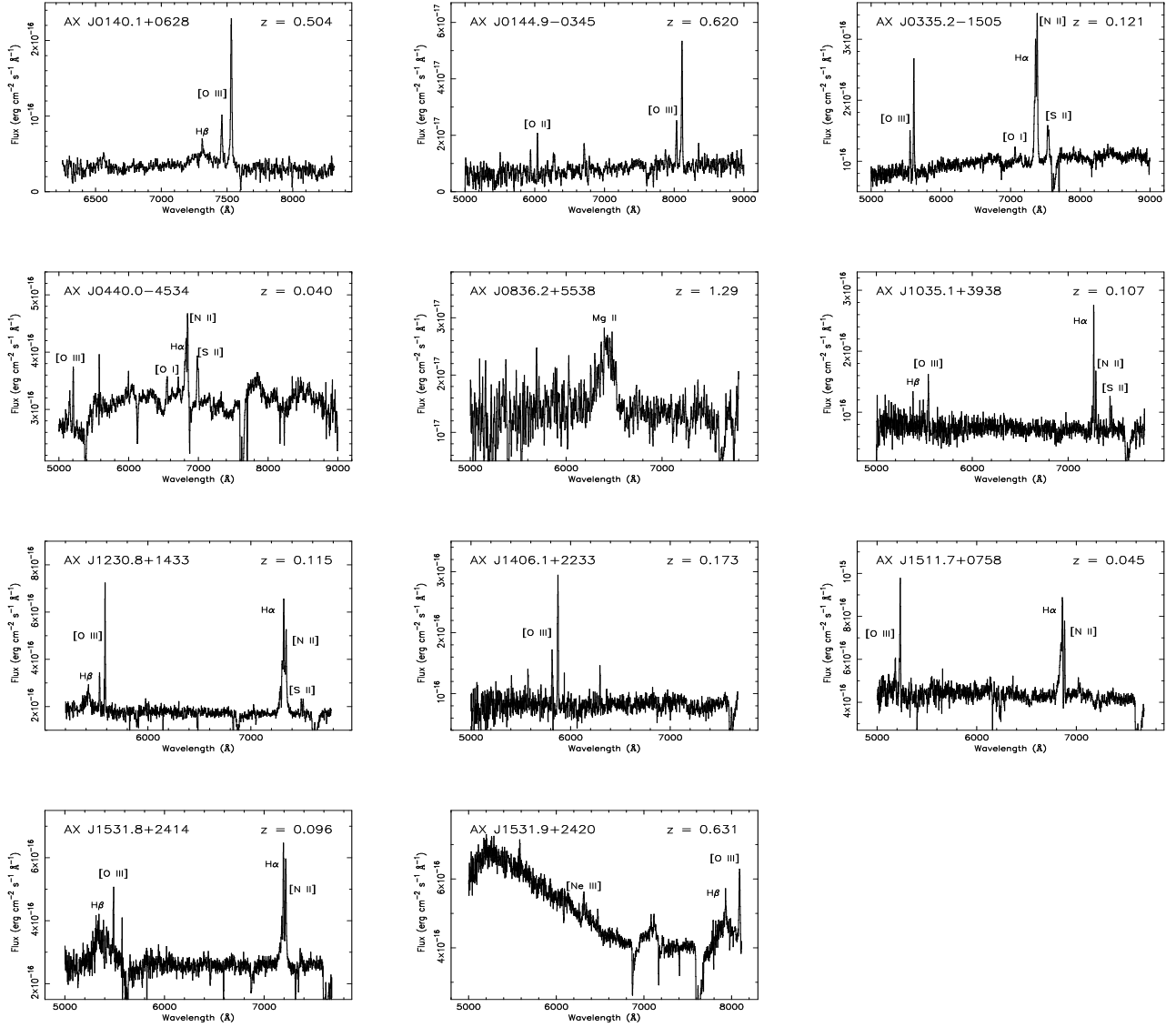


Figure 1. The optical spectra

name	ID <sup>1</sup>	z <sup>2</sup>	R <sup>3</sup>	B-R <sup>3</sup>	Extended <sup>4</sup>
AXJ0140.1+0628	BL	0.504	18.9	0.9	N
AXJ0144.9-0345	NL	0.620	20.1	2.4	N
AXJ0335.2-1505	NL	0.121	17.5	1.5	Y
AXJ0440.0-4534	NL	0.040	13.7	1.7	Y
AXJ0836.2+5538	BL	1.290	20.2	1.2	N
AXJ1035.1+3938	NL	0.107	18.1	1.4	Y
AXJ1230.8+1433	BL	0.115	16.7	1.4	Y
AXJ1406.1+2233	NL	0.173	17.7	2.0	Y
AXJ1511.7+0758	NL	0.045	15.3	1.2	Y
AXJ1531.8+2414	BL	0.096	16.9	1.7	Y
AXJ1531.9+2420	BL	0.631	17.2	0.5	N
AXJ1532.5+2415	-	-	19.6	2.3	N

<sup>1</sup> Spectral identification; <sup>2</sup> Redshift<sup>3</sup> Johnson R magnitudes and B-R colours<sup>4</sup> Optical Extension

Table 3. Optical Properties

fitting spectral slope ( $\Gamma = 2.4$ ) is steeper than the  $\Gamma = 1.9$  value that we used for the model fitting of the *Chandra* spectrum. When we leave the photon index free in the *Chandra* spectral fit we obtain  $\Gamma = 2.40^{+0.24}_{-0.13}$  with  $\chi^2 = 38.3/23$  in excellent agreement with *XMM-Newton*. The other source, AXJ1511.7+0758, is the less luminous in our sample. Its optical counterpart has a NL spectrum. The relatively low luminosity combined with the steep X-ray spectrum raises the possibility that a large fraction of the X-ray emission comes from star-forming processes. Thus we have added a Raymond-Smith component to the X-ray spectrum. The addition of this component significantly improves the fit ( $\chi^2 \approx 36.9/20$  for  $kT \approx 0.2$  keV). Leaving free the photon index as well results in a further improvement ( $\Delta\chi^2 \approx 5.3$ ). The best fit photon index becomes  $\Gamma = 1.46^{+0.22}_{-0.18}$ .

The absorbed flux estimates from the *Chandra* and *XMM-Newton* spectra are in agreement, except from the case of AXJ1230.8+1433, AXJ1406.1+2233, and AXJ1532.5+2415, which show a flux variation of the order of  $\sim 0.6$ , 2.5 and 3, respectively, between the *Chandra* and *XMM-Newton* observations. The two observations are separated by about 0.5, 10 and 13 months, respectively. The last object is still spectroscopically unidentified and hence we cannot estimate its luminosity. On the other hand, the other two objects are of moderate luminosity ( $3$  and  $9 \times 10^{43}$  erg  $s^{-1}$  respectively). Similar amplitude variations are observed in nearby BL objects on similar time scales. There is also a reasonable agreement, within the errors, between the *Chandra* and the *XMM-Newton*  $N_H$  best fitting values.

Most objects in the current sample show some amount of intrinsic absorption. Among the 11 objects with optical identifications, six are ‘‘absorbed’’ systems (i.e. they have a column density of  $> 10^{22}$   $\text{cm}^{-2}$ ). Nevertheless, five ‘‘soft’’, i.e.  $N_H < 10^{22}$   $\text{cm}^{-2}$ , sources can still be found in our sample. Sources AXJ1511.7+0758, AXJ1531.8+2414 and AXJ1531.9+2420 have not been observed by *ROSAT*. As they are soft bright sources, they would probably have been detected. Source AXJ1035.1+3938 was lying within the field-of-view (4.5 arcmin off-axis) of a *ROSAT* HRI pointing (1.7 ksec) but was not detected. Finally, source AXJ1230.8+1433 has been detected by *ROSAT* HRI.

In general, optically classified NL objects show more obscuration when compared to the BL objects. The median column density of the former class of objects in our sample is  $\sim 2 \times 10^{22}$   $\text{cm}^{-2}$ , compared to  $\sim 7 \times 10^{20}$   $\text{cm}^{-2}$  for the BL AGN. In fact, using a Kolmogorov-Smirnov test we find that the column density distribution of the NL and BL samples are different at the 87 per cent significance level. This is not a highly significant result (because of the small number of sources in our sample) but is nevertheless indicative that the trend we observe, i.e.  $N_{H,NL} > N_{H,BL}$ , may correspond to a real characteristic of the SHEEP sources. However, there are two clear exceptions to the general trend. The object which presents the highest X-ray obscuration is a BL AGN (AXJ0140.1+0628 at  $z=0.5$ ). Reversely, one of the objects with the lowest obscuration is a NL source at redshift of 0.045 (AXJ1511.7+0758).

Finally, there is a separation in redshift between BL and NL populations in our sample. The NL AGN are preferentially found at low redshifts (median redshift  $z=0.11$ ) while the BL AGN are in general located at higher distance having a median redshift of  $z=0.5$  (see Fig. 3). Applying the

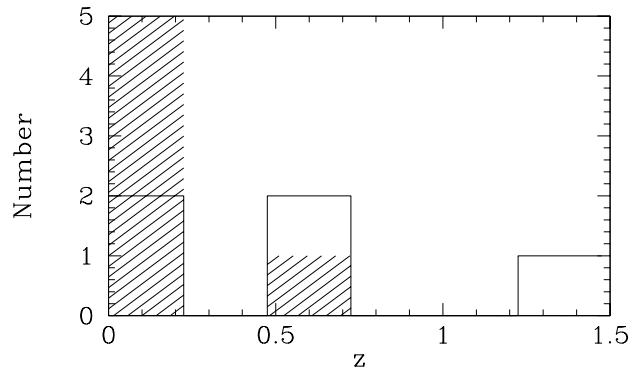


**Figure 3.** The redshift distribution of the BL (NL) AGN denoted with open (hatched) histogram.

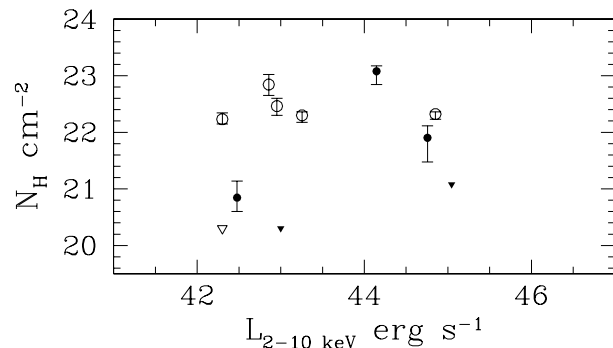


**Figure 4.** The column density derived from the *Chandra* spectral fits as a function of the 2-10 keV intrinsic luminosity. BL (NL) AGN are denoted with filled (open) symbols. The triangles denote upper limits. The errors correspond to the 90 per cent confidence level.

Wilcoxon, Mann, Whitney rank sum test, we find that the probability of BL objects having a median redshift larger than that of the NL objects is higher than 90%. Again, this is not a highly significant result, but it is highly suggestive that NL objects are rare at redshifts higher than  $\sim 0.3$ . Alternatively, as there is a tight correlation between redshift and luminosity in flux limited surveys, high luminosity sources, i.e.  $L_x > 10^{44}$  erg  $s^{-1}$ , appear to be associated primarily with BL AGN while the lower luminosity ones with NL AGN. The only highly luminous ( $L_x \sim 10^{45}$  erg  $s^{-1}$ ) NL object in our sample (AXJ0144.9-0345) has high column density ( $N_H > 10^{22}$   $\text{cm}^{-2}$ ) and thus is a candidate type II QSO.

name	$N_{H,Gal}^1$	counts	$\Gamma^2$	$N_H^3$	$\chi_\nu^2$	F(2-10) <sup>4</sup>	F(5-10) <sup>5</sup>	$L_x^6$	ID	z
AXJ0140.1+0628 <sup>a,c</sup>	4	47	1.9	$12^{+3}_{-5}$	-	1.9	1.3	14	BL	0.504
AXJ0144.9-0345	3	249	1.9	$2.1^{+0.2}_{-0.4}$	-	5.1	2.5	71	NL	0.620
AXJ0335.2-1505	5	124	1.9	$2.0^{+0.3}_{-0.5}$	-	4.0	2.0	1.8	NL	0.121
AXJ0440.0-4534 <sup>b</sup>	2	70	1.9	$1.7^{+0.5}_{-0.3}$	-	2.0	0.9	0.2	NL	0.040
AXJ0836.2+5538 <sup>b,c</sup>	4	89	1.9	$0.8^{+0.5}_{-0.8}$	-	1.0	0.45	57	BL	1.290
AXJ1035.1+3938 <sup>b,c</sup>	1	30	1.9	$7.0^{+3}_{-2.5}$	-	1.5	0.68	0.7	NL	0.107
AXJ1230.8+1433 <sup>a</sup>	2	172	1.9	$0.07^{+0.07}_{-0.03}$	-	1.2	0.54	0.3	BL	0.115
AXJ1406.1+2233 <sup>b</sup>	2	36	1.9	$2.9^{+1.1}_{-0.9}$	-	1.0	0.55	0.9	NL	0.173
AXJ1511.7+0758	2	407	$2.12^{+0.28}_{-0.20}$	< 0.02	52.0/23	2.3	1.0	0.2	NL	0.045
AXJ1531.8+2414	4	436	$2.42^{+0.21}_{-0.18}$	< 0.02	38.3/23	3.1	1.40	1.0	BL	0.096
AXJ1531.9+2420	4	759	$1.95^{+0.10}_{-0.09}$	< 0.02	50.7/40	6.0	2.70	111	BL	0.631
AXJ1532.5+2415 <sup>a</sup>	4	50	1.9	$1.6^{+0.6}_{-0.6}$	-	1.5	0.75	-	-	-

<sup>1</sup> Galactic column density in units  $10^{20} \text{ cm}^{-2}$ ;

<sup>2</sup> Photon index

<sup>3</sup> Intrinsic column density in units  $10^{22} \text{ cm}^{-2}$ ;

<sup>4</sup> Absorbed Flux (2-10 keV) in units  $10^{-13} \text{ erg cm}^{-2} \text{ s}^{-1}$ ;

<sup>5</sup> Absorbed Flux (5-10 keV) in units  $10^{-13} \text{ erg cm}^{-2} \text{ s}^{-1}$

<sup>6</sup> Intrinsic Luminosity (2-10 keV) in units  $10^{43} \text{ erg s}^{-1}$

<sup>a</sup> Observed and detected by ROSAT

<sup>b</sup> Observed but not detected by ROSAT

<sup>c</sup> Presented in Nandra et al. 2004

**Table 4.** The *Chandra* spectral fits

name	$N_{H,Gal}^1$	$\Gamma^2$	$N_H^3$	$\chi_\nu^2$	F(2-10) <sup>4</sup>	ID	z
AXJ0140.1+0628	4	1.9	$8.5^{+2.9}_{-2.6}$	25.5/22	1.3	BL	0.504
AXJ0836.2+5538	4	$1.73^{+0.19}_{-0.16}$	< 0.2	24.1/29	0.9	BL	1.290
AXJ1230.8+1433	2	1.9	< 0.02	-	0.7	BL	0.115
AXJ1406.1+2233	2	1.9	$3.2^{+1.0}_{-1.0}$	-	0.4	NL	0.173
AXJ1531.8+2414	4	$2.43^{+0.12}_{-0.08}$	< 0.02	79.1/90	2.8	BL	0.096
AXJ1531.9+2420	4	$2.14^{+0.07}_{-0.07}$	< 0.02	148.6/136	6.0	BL	0.631
AXJ1532.5+2415	4	1.9	$3.0^{+1.5}_{-1.1}$	-	0.5	-	-

<sup>1</sup> Galactic column density in units  $10^{20} \text{ cm}^{-2}$ ;

<sup>2</sup> Photon index

<sup>3</sup> Intrinsic column density in units  $10^{22} \text{ cm}^{-2}$ ;

<sup>4</sup> Absorbed Flux (2-10 keV) in units  $10^{-13} \text{ erg cm}^{-2} \text{ s}^{-1}$ ;

**Table 5.** The *XMM-Newton* spectral fits

## 4 DISCUSSION

Our survey provides a glimpse of bright, nearby examples of the hard AGN population which produces an appreciable fraction of the X-ray background. The subsample of the SHEEP survey presented here contains both Type I (BL) and Type II (NL) AGN, according to the optical classification.

Although the number of objects that we study is small, we find that there is a considerable difference in their redshifts, with NL objects preferentially found at redshifts lower than those of BL AGN. The cross-correlation of *GINGA* and *HEAO-1* X-ray background maps above 2 keV with nearby galaxy catalogues, demonstrates that an appreciable fraction of the hard X-ray emission may arise at low redshift,  $z \leq 0.1$  (Jahoda et al. 1991, Lahav et al. 1993). Our NL AGN clearly provide examples of this nearby AGN population. The distance separation between NL and BL AGN is ubiquitous in hard X-ray surveys with the redshift peak of the populations depending on the surveys's flux limit.

Our results are consistent with the hypothesis that NL AGN are, on average, less luminous than  $10^{44} \text{ erg s}^{-1}$ . Al-

though our statistics is clearly small, the same effect i.e. the NL AGN occupying preferentially the low luminosities, can be also witnessed in the *XMM-Newton* hard 4.5-7.5 keV sample of Caccianiga et al. (2004) which contains 28 sources. Five out of the seven NL AGN in Caccianiga et al. (2004) have 2-10 keV intrinsic luminosities lower than  $10^{44} \text{ erg s}^{-1}$ . Obviously, larger surveys are needed in order to confirm unambiguously that NL AGN are intrinsically less luminous than the BL AGN. For example, this could be the case in a scenario where highly luminous AGN (QSO) come preferentially in a "Broad Line flavour" in contrast to the low luminosity AGN (Seyferts) which appear as both NL or BL according to the viewing angle in respect to the obscuring torus. Steffen et al. (2003) find that the fraction of NL AGN decreases at high redshift,  $z > 1$ . Treister et al. (2004) observe the same effect but raise the criticism that this could be caused by incompleteness in the spectroscopic identification. Indeed luminous NL AGN at high redshift cannot be easily detected in the optical owing to large amounts of reddening (e.g. Fiore et al. 2003). The results emerging from our own survey as well as from that of Caccianiga et al.

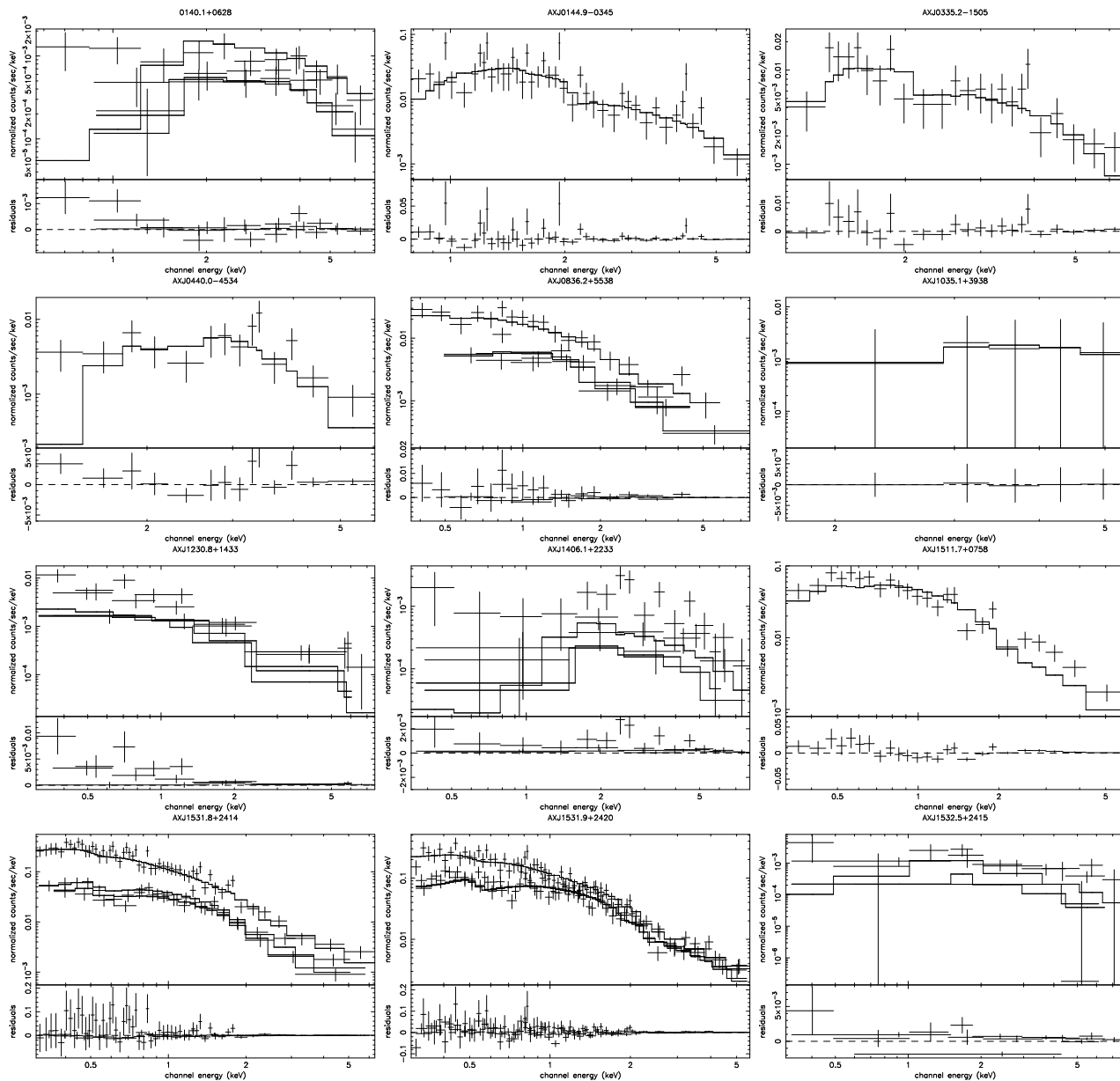


**Figure 2.** The X-ray spectra (*XMM-Newton* or *Chandra*) together with the best fit power-law model and the residuals (lower panels). Only the *XMM-Newton* spectra are presented (both the MOS and PN in the same panel) where available. In the case where the spectra have been fitted with C-statistic we bin the data to produce a signal to noise ratio of 10 for illustrative purposes

(2004), which has practically complete spectroscopic identification, lend support to the findings of Steffen et al. (2003). We note that the density of NL AGN in Steffen et al. (2003) decreases only at  $z > 1$ . A direct comparison of the redshift distribution of our sample with that of Steffen et al. is not straightforward as the flux limit of the latter sample is much deeper. Nevertheless, if the NL AGN are intrinsically fainter than the BL AGN, the effect is that the NL AGN are observed at lower redshifts compared with the BL ones in any given survey. Similarly, recent surveys (e.g. Barger et al. 2004) show evidence of “cosmic downsizing” where the low luminosity AGN have been formed at a later epoch compared with the bright QSOs. In particular, the peak of the redshift distribution of the low luminosity AGN peaks around  $z=0.7$ . Thus given that the NL AGN are low lumi-

nosity sources this provides an additional reason why these are observed at relatively low redshifts.

The column density distribution is almost equally divided between high and low column densities (table 4). In particular the fraction of sources with  $N_H > 10^{22} \text{ cm}^{-2}$  is  $58 \pm 22$  per cent. It has to be mentioned that we are dealing with a biased ‘hard’ sample since we have primarily observed with *Chandra*, the sources for which no *ROSAT* positions are available (ie those either not detected or not observed by *ROSAT*) and hence the above fraction should be only viewed as an upper limit. Therefore, our sample cannot provide a fair comparison with the X-ray background population synthesis models of e.g. Comastri et al. (2001). We note that Caccianiga et al. (2004) find a fraction of  $26 \pm 10$  for the fraction of obscured AGN, inconsistent with the predictions of

Comastri et al. (2001). We should be able to provide stronger constraints, when all the objects in the SHEEP survey have been observed by *Chandra*.

We find that NL objects are more obscured compared to BL objects, as expected from Unification models. However, there is a notable exception as the hardest source in the sample is associated with a BL AGN (0140.1+0628). The *XMM-Newton* spectrum presented here confirms the column density derived from the *Chandra* hardness ratio analysis (Nandra et al. 2004). The observed colour (B–R=0.8) suggests little absorption in the optical:  $A_V \approx 1.5$  assuming B–R=0.3 at  $z=0.5$  according to the SDSS QSO template spectrum of Vanden Berk et al. (2002). On the other hand the column density measured in the X-ray spectrum corresponds to  $A_V \sim 55$  assuming the Galactic dust-to-gas ratio (Bohlin, Savage & Drake 1978). This large discrepancy can be naturally explained by sublimation of the dust (eg Granato, Danese & Franceschini 1987). This may be the case in Broad-Absorption-Line (BAL) QSOs which usually present large absorbing column densities in the X-ray spectra, with typically  $N_H > 10^{23} \text{ cm}^{-2}$  (Gallagher et al. 2002), while they present moderate reddening in their colours (Brotherton et al. 2001). Actually, from the existing optical spectrum alone we cannot exclude the possibility that our object is a BAL. The most efficient diagnostic for the classification of a source as a BAL is the presence of a broad CIV line (1549 Å) which is outside the spectral window at the redshift of our object.

Finally, one the softest X-ray sources is associated with a NL source (AXJ1511.7+0758). It is puzzling why the optical reddening which should be responsible for the obliteration of the broad-line region does not produce significant absorption in X-rays. Typically, NL AGN (Seyfert-1.8-1.9.-2.0) present column densities higher than  $10^{23} \text{ cm}^{-2}$  (eg Awaki et al. 1991). One possibility is that at the low luminosity regime - our source has  $L_x \sim 10^{42} \text{ erg s}^{-1}$  - no broad-line region is formed (Nicastro 2000). Indeed, there are a few bona-fide examples of Seyfert-2 galaxies, (see Panessa & Bassani 2002, Georgantopoulos & Zezas 2003) with no obscuration in X-rays. Alternatively, the possibility that, at least, the X-ray emission comes primarily from star-forming processes cannot be ruled out. As discussed earlier the X-ray spectrum requires the presence of a soft thermal component. This would naturally explain the relatively low level of X-ray luminosity (see e.g. Zezas, Georgantopoulos & Ward 1998) as well as the soft X-ray spectrum. Nevertheless, the weak  $H\beta$  relative to the [OIII] line as well as the relative strength of the NII relative to the Ha suggest against the star-formation activity.

## 5 SUMMARY

We present *Chandra* and *XMM-Newton* observations of a subsample of 12 bright sources ( $f(2 - 10\text{keV}) > 10^{-13} \text{ erg cm}^{-2} \text{ s}^{-1}$ ) from the SHEEP *ASCA* 5-10 keV catalogue. We have obtained optical spectroscopic observations for 11 of these. The optical spectra show that our sources are associated with both NL and BL AGN. The X-ray spectra reveal intrinsic absorbing column densities of the order  $10^{20} - 10^{23} \text{ cm}^{-2}$ . The BL AGN on average do not present obscuration in X-rays compared to the NL AGN. There are however exceptions in this trend with the most obscured source being a

BL AGN. Although the statistics is limited, the NL AGN are found at lower redshift and luminosity compared with the BL sources. The most likely explanation is that NL AGN are intrinsically less luminous than the BL ones and thus they are preferentially found at lower redshifts.

## 6 ACKNOWLEDGMENTS

This work is funded by the Greek National Secretariat for Research and Technology in the framework of the Programme Participation in Projects of International Organisations (European Space Agency). We also acknowledge support by the European Union and the Greek Ministry of Development in the framework of the programme 'Promotion of Excellence in Technological Development and Research', project 'X-ray Astrophysics with ESA's mission XMM'. We acknowledge the use of data from the *XMM-Newton* Science Archive at VILSPA. Skinakas Observatory is a collaborative project of the University of Crete, the Foundation for research and Technology-Hellas, and the Max-Planck-Institut für Extraterrestrische Physik.

## REFERENCES

- Alexander D., et al., 2003, *AJ*, 126, 539  
 Arnaud, K., 1996, *PASP Conference Series*, 101, p. 17  
 Awaki, H., Koyama, K. Inoue, H., Halpern, J.P., 1991, *PASJ*, 43, 195  
 Bohlin, R.C., Savage, B.D., Drake, J.F., 1978, *ApJ*, 224, 132  
 Brotherton, M.S., Tran, H.D., Becker, R.H., Gregg, M.D., Laurent-Muehleisen, S.A., White, R.L., 2001, *ApJ*, 546, 775  
 Caccianiga, A., et al. 2004, *A&A*, 416, 901  
 Cash, W., 1979, *ApJ*, 228, 939  
 Comastri, A., Setti, G., Zamorani, G., Hasinger, G., 1995, *A&A*, 296, 1  
 Comastri, A., Fiore, F., Vignali, C., Matt, G., Perola, G. C., La Franca, F., 2001, *MNRAS*, 327, 781  
 Dickey, J.M., & Lockman, F.J., 1990, *ARA&A*, 28, 215  
 Fiore, F., La Franca, F., Giommi, P., Elvis, M., Matt, G., Comastri, A., Molendi, S., Gioia, I. 1999, *MNRAS*, 306, L55  
 Fiore, F. et al., 2003, *A&A*, 409, 65  
 Gallagher, S.C., Brandt, W.N., Chartas, G., Garmire, G.P., 2002, *ApJ*, 567, 37  
 Gendreau, K. et al. 1995, *PASJ*, 47, L5  
 Georgakakis, A., Georgantopoulos, I., Akylas, A., 2005, *MNRAS*, submitted  
 Georgantopoulos, I. & Zezas, A., 2003, *ApJ*, 594, 704  
 Georgantopoulos, I., Georgakakis, A., Akylas, A., Stewart, G.C., Giannakis, O., Shanks, T., Kitsionas, S., 2004, *MNRAS*, 352, 91  
 Giacconi R., et al., 2002, *ApJS*, 139, 369  
 Gilli, R., Salvati, M., Hasinger, G., 2001, *A&A*, 366, 407  
 Granato, G.L., Danese, L., Franceschini, A., 1987, *ApJ*, 486, 147  
 Jahoda, K., Mushotzky, R.F., Boldt, E., Lahav, O., 1991, *ApJ*, 378, L37  
 Lahav, O., et al. 1993, *Nature*, 364, 693  
 Nandra, Georgantopoulos, I., Ptak, A., Turner, T.J., 2003, *ApJ*, 582, 615  
 Nandra, K., Georgantopoulos, I., Brotherton, M., Papadakis, I., 2004, *MNRAS*, 347, L41  
 Nicastro, F., 2000, *ApJ*, 530, L65  
 Panessa, F., Bassani, L., 2002, *A&A*, 394, 435  
 Perola, G.C. et al. *A&A*, 421, 491



- Piconcelli, E., Cappi, M., Bassani, L., Fiore, F., Di Cocco, G.,  
Stephen, J.B., 2002, A&A, 394, 835
- Steffen, A.T., Barger, A.J., Cowie, L.L., Mushotzky, R.F., Yang,  
Y., 2003, ApJ, 596, L23
- Strüder L., Briel U., Dennerl K., et al. 2001, A&A, 365, L18.
- Tozzi, P. et al., 2001, ApJ, 562, 42
- Treister, E., et al. 2004, ApJ, 616, 123
- Turner M. J. L., Abbey A., Arnaud M., et al., 2001, A&A, 365,  
L27.
- Watanabe, S., Akiyama, M., Ueda, Y., Ohta, K., Mushotzky, R.,  
Takahashi, T., Yamada, T., 2002, PASJ, 54, 683
- Van den Berk, D.E., et al. 2001, AJ, 122, 549
- Weisskopf, C., 1997, Astroph. Lett. & Comm., 26, 1
- Zezas, A., Georgantopoulos, I., Ward, M.J., 1998, MNRAS, 301,  
915